OPTIMUM SPECTRAL RESOLUTION FOR COMPUTING ATMOSPHERIC HEATING AND PHOTODISSOCIATION RATES

K. STAMNES

Geophysical Institute and Department of Physics, University of Alaska,
Fairbanks, AK 99775-0800, U.S.A.

and

S.-C. TSAY

Department of Atmospheric Science, Colorado State University, Fort Collins, CO 80523, U.S.A.

Abstract—Rapid, reliable and accurate computations of atmospheric heating rates are needed in climate models aimed at predicting the impact of greenhouse gases on the surface temperature. Photolysis rates play a major role in photochemical models used to assess potential changes in atmospheric ozone abundance due to man's release of chlorofluorocarbons. Both rates depend directly on the amount of solar radiation available at any level in the atmosphere. We present a very efficient method of computing these rates in which integration over the solar spectrum is reduced to a minimum number of monochromatic (or pseudo-gray) problems by appealing to the continuum features of the ozone absorption cross-sections.

To explore the resolutions needed to obtain adequate results we have divided the spectral range between 175 and 700 nm into four regions. Within each of these regions we may vary the resolution as we wish. Accurate results are obtained for very coarse spectral resolution provided all cross-sections are averaged by weighting them with the solar flux across any bin. By using this procedure we find that heating rate errors are less than 20% for all altitudes when only four spectral bands across the entire wavelength region from 175 to 700 nm are used to compute the heating rate profile. Similarly, we find that the error in the photodissociation of ozone is less than a few percent when 10 nm resolution is used in the Hartley and Huggins bands (below 330 nm), while an average over the entire wavelength region from 400 to 700 nm yields similar accuracy for the Chappuis band. For integrated u.v. dose estimates a resolution slightly better than 10 nm is required in the u.v.B region (290–315 nm) to yield an accuracy better than 10%, but we may treat the u.v.A region (315–400 nm) as a single band and yet have an accuracy better than 2%.

1. INTRODUCTION

In climate models aimed at predicting the impact of greenhouse gases on surface temperature, the atmospheric heating rate must be determined. Likewise, in photochemical models the photodissociation rates of the various gases involved in the atmospheric chemistry, are of paramount importance for correct assessments of potential changes in atmospheric ozone amount due to natural or anthropogenic causes. Both rates depend directly on the amount of radiation available at any level in the atmosphere. Thus, in two- and three-dimensional climate or photochemical models the radiation field needs to be determined many times over the spatial and temporal domains. This implies that radiative transfer calculations must be performed repeatedly; in fact, they could easily consume the lion's share of available computer resources. Since the heating rate as well as the photodissociation rate are proportional to moments of the radiation field, there is a need for fast computation of the flux divergence or the mean intensity at a given level in the atmosphere.

This situation has led to highly parameterized treatments of solar radiation in two- and three-dimensional climate models as well as in photochemical models. There is nothing wrong in principle with such an approach, but it would be desirable to have available a fast method for direct computation of the radiation field for the following reason: most parameterized treatments of atmospheric radiation in large-scale models are not well suited to undertake studies of the impact of clouds on their performance and predictions. Even in one-dimensional climate models the microphysics of clouds cannot be properly simulated (Liou and Ou, 1989). Yet clouds constitute

one of the least understood elements of the climate system, and it has recently been suggested that cloud microphysics may play a major role in climate response to radiation forcings such as a carbon dioxide doubling (Liou and Ou, 1989). In fact, model calculations based on measured cloud microphysics in the Arctic, showed that cloud radiative properties are indeed sensitive to cloud microphysical properties (Tsay *et al.*, 1983). Also, the impact of clouds on the photochemistry in the troposphere as well as the stratosphere (polar stratospheric clouds) has not been thoroughly or systematically investigated.

Rapid, reliable and accurate computation of the transfer of radiation in the atmosphere is desirable for yet another important reason: to assess biological u.v. doses for various ozone depletion scenarios anticipated to be the consequence of continued release of man-made pollution (NASA, 1988), appropriate radiative transfer models are of utmost importance (cf. e.g. Dahlback *et al.*, 1989). Such models will also play a key role in distinguishing the impact on u.v. dose caused by changes in ozone from that due to other environmental parameters including possible alterations in cloud cover and aerosol loading (Fredrick and Lubin, 1988; Scotto *et al.*, 1988; Stamnes *et al.*, 1988a) as well as in assessing the effects of changes in the vertical distribution of atmospheric ozone on the amount of u.v. radiation received by the biosphere (Bruhl and Crutzen, 1989). Finally, we expect radiative transfer modeling to become an indispensable tool for predicting u.v. penetration into the ocean and thereby enabling us to assess possible harmful effects of an ozone depletion on marine ecosystems.

In this paper we shall discuss a direct computation of the atmospheric radiation field in a stratified atmosphere in which aerosol and cloud microphysical properties can be taken explicitly into account. For such a computation to be both efficient and accurate we must choose the wavelength grid over the solar (u.v. and visible) spectrum judiciously, and take the vertical inhomogeneity of the atmosphere properly into account. Here we want to address the first item, namely the proper choice of wavelength grid to make our computations as rapid as possible for a specified level of desired accuracy. Our aim is to reduce the integration over the solar spectrum to a series of N monochromatic (or "pseudo-gray") problems with N as small as possible. Each monochromatic radiative transfer problem can be solved with a variety of techniques (cf. e.g. Stamnes, 1986, for a review). A four-stream calculation based on the state-of-the-art discrete ordinate algorithm described by Stamnes *et al.* (1988b) will be adopted here because of its computational efficiency and reliability.

2. DESCRIPTION OF THE MODEL

2.1. *General*

We have recently constructed a comprehensive radiation model for solar and terrestrial radiation (Tsay *et al.*, 1989, 1990). In this model integrations over spectral bands for which Beer's law does not apply, were reduced to a series of monochromatic computations by employing the so-called exponential-sum-fitting-of-transmission functions (ESFT) technique. In the paper by Tsay *et al.* (1990) we showed that while this approach yields adequate heating rates in the troposphere, its validity in the stratosphere is questionable because the ESFT-technique, as commonly practiced, requires empirical pressure and temperature scaling of the absorber amount. Scaling is generally required to take into account the pressure and temperature dependence of the absorption line profile with altitude, but should not be needed in the spectral range considered here, since the ozone absorption bands show continuum features. In fact, we show in this paper that such scaling is inadequate for the ozone absorption bands in the u.v. and visible part of the solar spectrum. The temperature dependence of the ozone absorption cross-section has been measured (cf. e.g. Molina and Molina, 1986). This dependence can be easily included into a model such as the present one, but the effect on heating and photolysis rates will be small compared with other uncertainties in our knowledge of the atmosphere affecting the computed radiation field.

The absorption cross-section for most absorbing atmospheric gases (e.g. water vapor, carbon dioxide and ozone) in the near-infrared part of the solar spectrum (longwards of 700 nm) and throughout the terrestrial spectrum (longwards of 4000 nm) varies rapidly but also very erratically with wavelength. The ESFT-technique and its closely related cousin the so-called k-distribution method (cf. Goody and Yung, 1989, for a review) are designed to cope with this erratic behavior of the absorption cross-section across a finite spectral interval. Thus, the merit of these techniques is essentially to reduce the radiative transfer problem involving integration over a finite spectral interval (for which Beer's law does not apply) to a series of monochromatic problems by approximating the transmission function for the interval with a sum of exponential functions. However, except for some line structure of the ozone absorption in the Huggins band in the vicinity of 320 nm, the cross-sections for ozone and molecular oxygen absorption in the u.v. and visible spectral range between 175 and 700 nm are generally smooth functions of wavelength. Hence, we may define proper averages over wide spectral

intervals such that Beer's law holds approximately over any such interval. How to define such an average will be discussed in Section 2.3.

2.2. *Basic equations*

To compute heating and photodissociation rates we need only integrated quantities such as the flux (irradiance) or the mean intensity of the radiation field as defined below. Therefore, we start with the azimuthally averaged version of the equation describing the transfer of diffuse monochromatic radiation at wavelength λ in a scattering, absorbing plane-parallel atmosphere given by (Chandrasekhar, 1960; Stamnes, 1986)

$$\mu \frac{\mathrm{d}u_\lambda(z,\mu)}{n(z)\,\mathrm{d}z} = -[\sigma_{\mathrm{abs}}(\lambda) + \sigma_{\mathrm{sca}}(\lambda)]u_\lambda(z,\mu)$$

$$+ \frac{\sigma_{\mathrm{sca}}(\lambda)}{2} \int_{-1}^{1} P_\lambda(\mu;\mu')u_\lambda(z,\mu')\,\mathrm{d}\mu'$$

$$+ \frac{\sigma_{\mathrm{sca}}(\lambda)I_{0,\lambda}}{4\pi} P_\lambda(\mu;-\mu_0)\,\mathrm{e}^{-\tau_\lambda(z)/\mu_0}. \quad (1)$$

Here z is the geometric altitude, θ is the polar angle and $\mu = \cos\theta$. We have made the usual diffuse-direct distinction (Chandrasekhar, 1960, p. 22) so that u_λ in equation (1) describes the azimuthally averaged diffuse intensity or radiance only. Thus, $I_{0,\lambda}$ is the intensity of solar radiance incident in direction μ_0 so that $\mu_0 I_{0,\lambda}$ is the incident vertical flux or irradiance. Furthermore, $\sigma_{\mathrm{abs}}(\lambda)$ and $\sigma_{\mathrm{sca}}(\lambda)$ are the absorption and scattering cross-sections, $P_\lambda(\mu;\mu')$ the azimuthally averaged phase function, and $\tau_\lambda(z)$ the extinction optical depth. The second term on the right side in equation (1) is due to multiple scattering, while the third is a consequence of the diffuse-direct distinction and is called the solar pseudo-source. Note that we have for simplicity written equation (1) for a single-constituent atmosphere with number density $n(z)$. Generalizing it to a multi-constituent medium is easily achieved by summing over constituents. The results reported in Section 3 pertain to a multi-constituent atmosphere.

By dropping the solar pseudo-term in equation (1), so that $u(z,\mu)$ refers to the total diffuse plus direct intensity, and then integrating over solid angles, we find the following relation between the flux (F) and the mean intensity ($\tilde{I}$) (cf. e.g. Stamnes, 1986):

$$\frac{\mathrm{d}F(z)}{\mathrm{d}z} = -4\pi n(z)\sigma_{\mathrm{abs}}\tilde{I}(z), \quad (2)$$

where we have dropped the λ-subscripts and

$$F(z) = 2\pi \int_{-1}^{1} \mu u(z,\mu)\,\mathrm{d}\mu \quad (3)$$

and

$$\tilde{I}(z) = \frac{1}{2} \int_{-1}^{1} u(z,\mu)\,\mathrm{d}\mu. \quad (4)$$

Heating rates may be computed from equation (2) in units of energy per unit volume per unit time or else by the formula

$$C_{\mathrm{p}} \frac{\partial T(z)}{\partial t} = -\frac{1}{\rho} \frac{\partial F(z)}{\partial z}, \quad (5)$$

in units of energy per unit mass per unit time. In equation (5), ρ is the mass density and C_{p} the specific heat at constant pressure. It has been customary to refer to

$$\frac{\partial T(z)}{\partial t} = -\frac{1}{C_{\mathrm{p}}\rho} \frac{\partial F(z)}{\partial z}$$

(in units of degrees per unit time) as the heating rate (cf. e.g. Liou, 1980). Since it is actually the rate of temperature change, we propose here to use the term "warming rate" and reserve the term heating rate for the quantity with the proper units in an attempt to avoid misleading and confusing terminology. This is consistent with the term cooling rate which is already in frequent use for terrestrial radiation. Finally, photodissociation rates may be computed by the formula (e.g. Brasseur and Solomon, 1984; Madronich, 1987)

$$J_i(z) = 4\pi \int_0^\infty q_i(\lambda)\sigma_i(\lambda)\tilde{I}(\lambda)\,\mathrm{d}\lambda, \quad (6)$$

where $q_i(\lambda)$ is the quantum efficiency and $\sigma_i(\lambda)$ the photoabsorption cross-section for species denoted by i.

Before proceeding we note that the units of the radiance, u_λ, in equation (1) are the same as those of $I_{0,\lambda}$, the units of which may be watts per unit area per unit steradian per unit wavelength interval. We note, however, that for the computation of photolysis rates by equation (6) the radiance must be in units of photons per unit area per unit time per unit steradian per unit wavelength interval.

2.3. *Averaging procedure: the Chandrasekhar mean*

Once we have chosen a grid (or wavelength bin size) to perform the integration over the solar spectrum, the integral in equation (6) is replaced by a discrete sum. It is then of great importance to choose the wavelength grid in such a way that this integral is accurately evaluated for as coarse a grid as possible, since we are keenly interested in computational efficiency. The important point to notice here is that accurate evaluations of heating and photodissociation

rates depend crucially on our ability to compute F and $\tilde{I}$ correctly and subsequently the integral in equation (6) by summation. Hence, a consistent computation of heating and photodissociation rates requires a proper procedure for averaging over the bin size.

In Fig. 1 we have plotted the cross-sections for ozone and molecular oxygen adopted here together with the extraterrestrial solar flux. These cross-section data were taken from a compilation recommended for use in aeronomical applications (WMO, 1985), while the solar flux data are from a recent compilation by Nicolet (1989). The cross-section for molecular oxygen in Fig. 1 includes only the Herzberg continuum in the spectral range 175–200 nm. Although the major absorption here is the Schumann–Runge bands, this band system is omitted from consideration in this paper for reasons given in Section 4. To explore the effect of the spectral resolution on the achieved accuracy, these cross-section and solar flux data were aver-
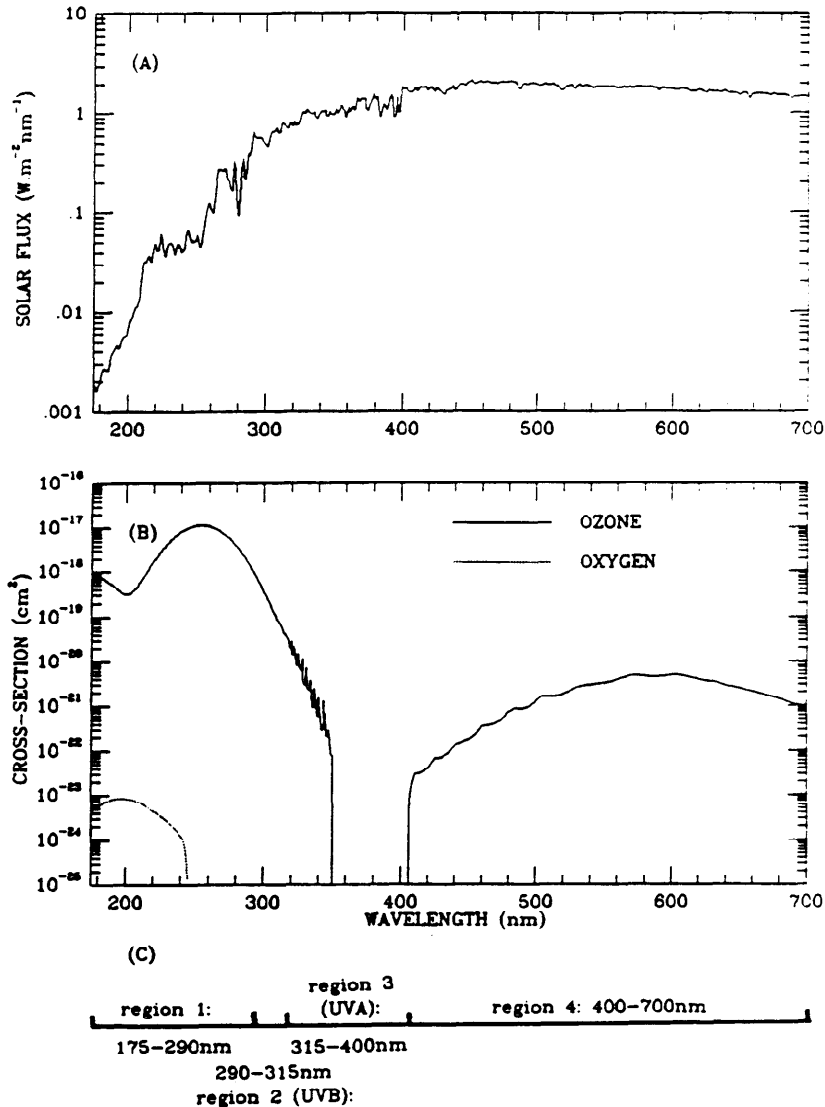
FIG. 1. (A) SOLAR FLUX AT THE TOP OF THE ATMOSPHERE, (B) ABSORPTION CROSS-SECTIONS FOR MOLECULAR OXYGEN (DOTTED LINE) AND OZONE (SOLID LINE), AND (C) ILLUSTRATION OF SPECTRAL REGIONS CONSIDERED (SEE TEXT).

aged to 1 nm resolution between 175 and 700 nm. This allows us to compare results computed with different resolutions, while computations made with 1 nm resolution may be regarded as benchmark. We have for convenience divided the total spectral range (175–700 nm) considered here into four separate regions as indicated in Fig. 1C. Within each of these regions we may vary the resolution as we wish. In region 1 (175–290 nm), where the ozone absorption cross-section peaks, there is overlapping between O_2 and O_3 absorption. Region 2 covers the u.v.B range from 290 to 315 nm where the ozone absorption decreases rapidly with wavelength, and region 3 covers the u.v.A range from 315 to 400 nm. Finally, region 4 extends from 400 to 700 nm which includes the relatively weak absorption band in the visible called the Chappuis band.

In order to evaluate the integral in equation (6) by a discrete sum a proper averaging procedure must be invoked; because of the rapid (although smooth) variation of the absorption cross-sections with wavelength (cf. Fig. 1), we should avoid using the arithmetic mean of the cross-section for any bin, but rather define an average cross-section by weighting it with the solar flux across that bin as follows (Chandrasekhar, 1960):

$$\sigma_{ave} = \frac{\int_{\lambda_1}^{\lambda_2} \sigma(\lambda) I_{0,\lambda} \, d\lambda}{\int_{\lambda_1}^{\lambda_2} I_{0,\lambda} \, d\lambda}, \quad (7)$$

where the bin considered lies between wavelengths λ_1 and λ_2. It is important that all the cross-sections used in equations (1)–(6) above be weighted in this manner. Thus, in equation (1) we need to define an average value for the absorption and scattering cross-sections by applying equation (7) to each of them, and in equation (6) the photoabsorption cross-section, $\sigma_i(\lambda)$, and the quantum efficiency, $q_i(\lambda)$, must be similarly averaged.

3. RESULTS

In order to be specific we chose to make our computation for a standard U.S. midlatitude atmosphere, although the choice of atmospheric model is irrelevant for the points we want to make in this paper. Figure 2 shows the vertical profile of the ozone concentration. The atmosphere is divided into 40 layers from sea level to 80 km height with an even spacing of 2 km in our computations and the integrated column ozone amount is 347.36 DU.

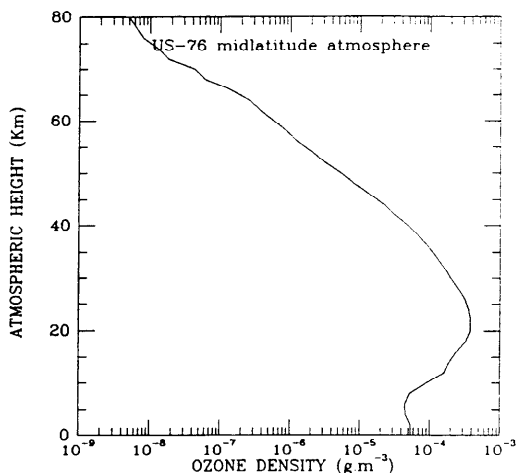Scattering by air molecules (Rayleigh scattering) is

FIG. 2. OZONE DENSITY PROFILE FOR U.S. STANDARD ATMOSPHERE ADOPTED IN THIS STUDY.

also taken into account by adopting the Rayleigh scattering cross-section from the WMO (1985) compilation. The surface albedo throughout the spectral range of interest is taken to be 20% which is close to a climatological mean value for continental vegetation (Kondratyev, 1969, p. 425).

The following results are obtained by arbitrarily choosing a solar zenith angle of 55°. Computations for different zenith angles generally produced similar results. To achieve adequate accuracy for our comparisons, we adopted a four-stream approximation to the radiative transfer equation based on the discrete-ordinate-method algorithm described by Stamnes et al. (1988b). We have previously published quite extensive validations of our model computations, and comparisons with the work of others are provided most recently by Tsay et al. (1990). The importance of doing these calculations correctly in connection with photochemical modeling has been discussed elsewhere with emphasis on the effects of multiple scattering and ground reflection (e.g. Luther and Gelinas, 1976; Meier et al., 1982; Nicolet et al., 1982) as well as the profound influence of clouds (e.g. Madronich, 1987).

3.1. Warming rates

In Fig. 3 we show the computed warming rates for the four spectral intervals defined in Fig. 1 and for different spectral resolutions. Note that the scales of the abscissas are different for the various panels. As expected, the largest heating occurs in region 1 (175–290 nm) where the cross-section peaks (Fig. 1). We observe that for regions 1, 2 and 3 (i.e. below 400 nm)
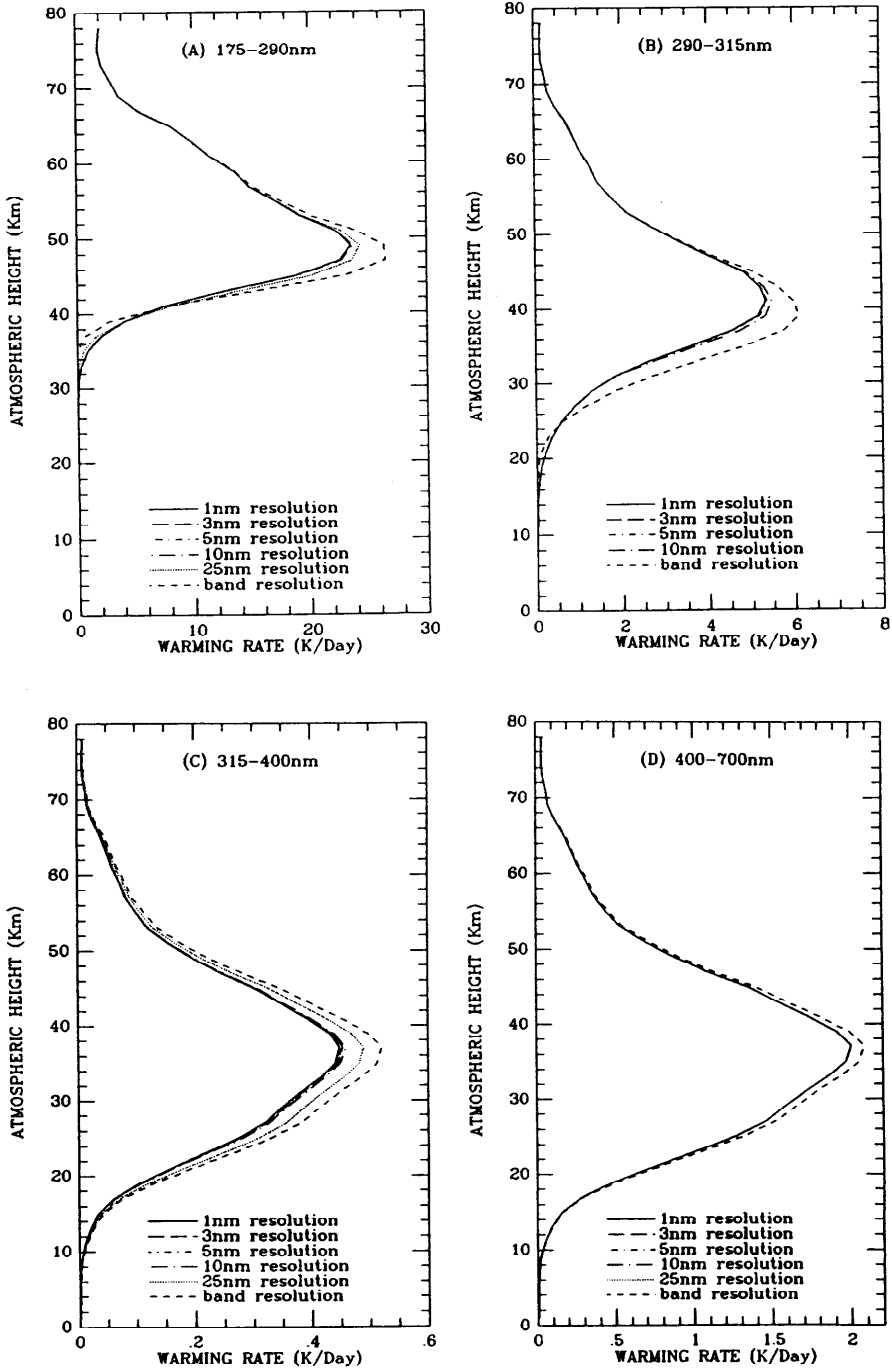
FIG. 3. ATMOSPHERIC WARMING RATES FOR THE SPECTRAL INTERVALS SHOWN IN FIG. 1C FOR VARIOUS SPECTRAL RESOLUTIONS; (A) REGION 1: 175–290 nm, (B) REGION 2: 290–315 nm (U.V.B), (C) REGION 3: 315–400 nm (U.V.A), AND (D) REGION 4: 400–700 nm (CHAPPUIS BAND).

resolutions of 1, 3 and 5 nm yield very similar results. Figure 3B indicates that in the u.v.B region a resolution of 10 nm may be acceptable if a maximum error in the total warming rate of about 0.2 K is tolerated around 40 km. Moreover, Fig. 3C shows that an error of similar magnitude is incurred by averaging over the entire u.v.A region (315–400 nm). Finally, we observe from Fig. 3D that 25 nm resolution yields excellent results for the Chappuis band; in fact, averaging over the entire region (400–700 nm) may give adequate results for most purposes since the contribution to the warming rate from the Chappuis band is in any case very small. We notice also from Fig. 3 that the contributions to the warming rate from the different regions peak at progressively lower altitudes with increasing wavelength. This behavior is consistent with Fig. 2 and expected from Fig. 1, since the cross-section decreases markedly with wavelength.

Figure 3 and detailed tabular results (not shown here) may be used to examine the relative error as a function of resolution by using the 1 nm result as a benchmark. Thus, we observe that even a resolution as coarse as 25 nm below 290 nm yields an error in the warming rate less than 10% in the 45–50 km region where the maximum heating occurs. Although the error is large below 40 km for 25 nm resolution, this is of little consequence because the heating below 40 km is dominated by radiation in the u.v.B region. Inspection of the tabular results confirms our previous inference based on Fig. 3 that a 10 nm resolution may be acceptable in the u.v.B region, since it leads to errors less than 5% where the major portion of the heating caused by u.v.B radiation occurs (between 45 and 35 km). Similarly, we infer that if an error of about 10% is tolerated between 30 and 40 km where most of the heating due to u.v.A radiation occurs (cf. Fig. 3C), then a resolution of 25 nm is acceptable in this region. Since relatively little heating takes place in this wavelength range a 10% error may be acceptable. Finally, Fig. 3D shows that we may average over the entire Chappuis band (400–700 nm) without making errors greater than 5%.

In climate modeling, the radiative forcings are often discussed in terms of the changes in the fluxes at top and bottom boundaries. Table 1 shows the computed upward flux at the top and the downward flux at the bottom of the atmosphere for different spectral resolutions. In addition to the four spectral ranges introduced previously (cf. Fig. 1), we also show results for one three-band model and two two-band models defined as follows: 3-band (175–290, 290–400, 400–700 nm), 2-band-B (175–315, 315–700 nm) and 2-band-A (175–400, 400–700 nm). Table 1 indicates that except for the 2-band-A model which divides the spectrum into two bands at 400 nm, all the other spectral divisions produce accurate values for the reflected and the transmitted fluxes. To investigate the spectral resolution required to obtain acceptable warming rates, we plotted profiles of computed warming rates for different spectral resolutions in Fig. 4A, and the corresponding errors with respect to the 1 nm calculation in Fig. 4B. We see that if errors no larger than 20% are acceptable, the four-band model (cf. Fig. 1) yields adequate results. This means that we have reduced the wavelength integration from 175 to 700 nm to four effective monochromatic calculations by using the Chandrasekhar mean [equation (7)] to average the cross-sections in each of the spectral regions defined in Fig. 1.

Comparing Table 1 and Fig. 4 we see that the 2-band-B model, which yields accurate fluxes at the top and bottom boundaries, leads to warming rate errors as large as 100% in the stratosphere, while the 2-band-A model yields even worse results. This shows that it can be very deceiving to check results only at the boundaries if one is also interested in warming rate profiles and the resulting dynamical effects.

3.2. Comparison with the ESFT technique

In Table 2 and Figs 5 and 6 we show a comparison

TABLE 1. COMPUTATIONS OF REFLECTED FLUX AT THE TOP AND TRANSMITTED FLUX ($W\ m^{-2}$) AT THE BOTTOM WITH OXYGEN AND OZONE ABSORPTION AND RAYLEIGH SCATTERING FOR DIFFERENT SPECTRAL RESOLUTIONS (SEE TEXT FOR DEFINITION); VALUES IN PARENTHESES ARE RELATIVE ERRORS WITH RESPECT TO RESULTS OF 1 nm RESOLUTION

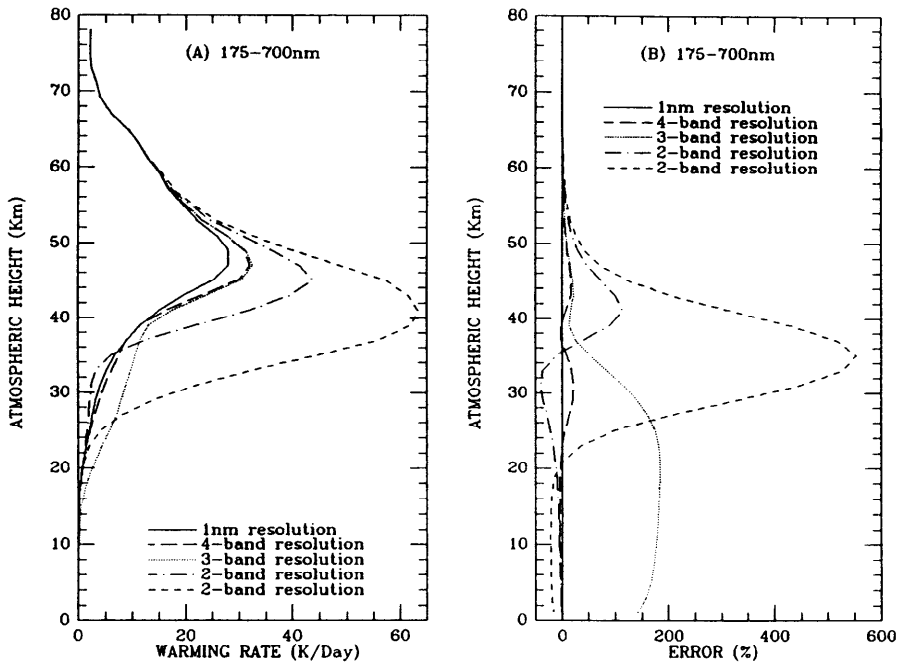|	1 nm	25 nm	4-band	3-band	2-band-B	2-band-A
Top	98.02	97.54	97.54	97.51	99.35	76.00
	—	(−0.5%)	(−0.5%)	(−0.5%)	(+1.4%)	(−22.5%)
Bottom	312.16	311.37	310.38	310.37	307.98	273.18
	—	(−0.3%)	(−0.6%)	(−0.6%)	(−1.3%)	(−12.5%)

FIG. 4. (A) Warming rates for the entire spectral region (175–700 nm) considered in this study for various spectral resolutions and (B) corresponding errors (see text).

between the ESFT technique for computing warming rates and our present procedure based on averaging the cross-sections by weighting them with the solar flux. The particular ESFT model used is described by Tsay et al. (1989, 1990). The set of exponential-sum-fitting coefficients adopted here (cf. Tsay et al., 1990) corresponds to reducing the wavelength integration from 175 to 700 nm to about 120 monochromatic computations. Inspection of Table 2 and Figs 5 and 6 reveals the following results:

(1) Pressure and temperature scaling of the absorber amount is definitely inappropriate for the

ozone absorption in the u.v. and visible region of the spectrum. Figure 6 shows that such scaling yields very poor results both in the troposphere and the stratosphere.

(2) The ESFT-technique without scaling yields very reasonable heating rates throughout the troposphere and stratosphere.

(3) While the ESFT-technique (without scaling) performs somewhat better between 35 and 55 km, the four-band model is superior at all other altitudes. This is very satisfying in view of the fact that our four-band model is more than 10 times faster than the ESFT model (cf. Fig. 7 and discussion to follow).

Since computational efficiency is a matter of major concern in large models, we show in Fig. 7 how the CPU time varies with resolution. We see that the ESFT model is about 10 times slower than the four-band model (both of which yields adequate results). While the ESFT model is based on precomputed "absorption" coefficients, the averaging of the cross-sections in the four-band model is done during the run. Thus, if the average absorption cross-sections were precomputed, the four-band model would be even faster than shown in Fig. 7.
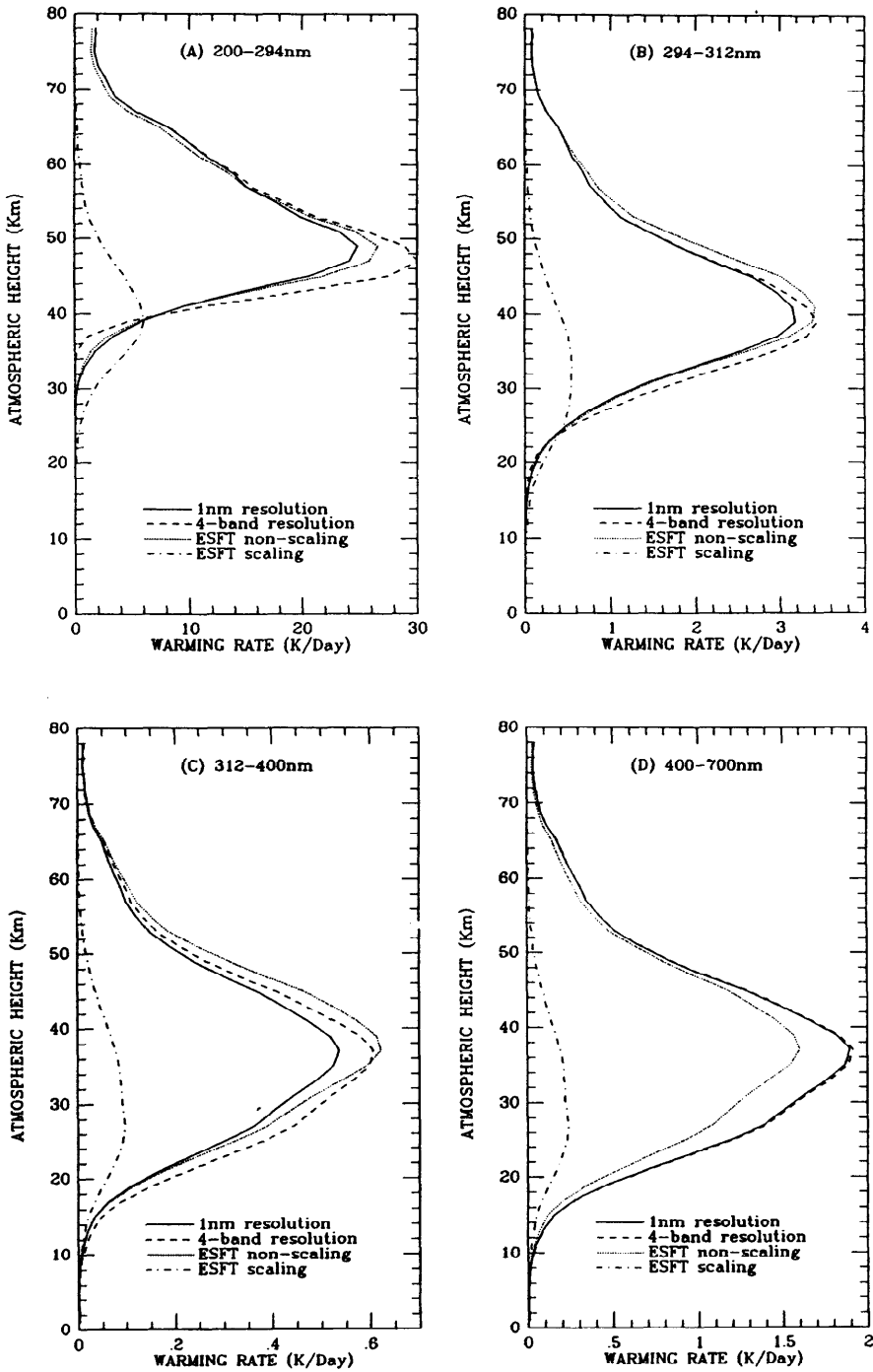
TABLE 2. COMPUTATIONS OF REFLECTED FLUX AT THE TOP AND TRANSMITTED FLUX (W m^{-2}) AT THE BOTTOM WITH OZONE ABSORPTION ONLY FOR SPECTRAL RANGE OF 200–700 nm, BASED ON THE PRESENT METHOD (1 nm AND 4-BAND) AND THE ESFT METHOD (WITH AND WITHOUT SCALING)

	1 nm	4-band	ESFT/ no scaling	ESFT/ scaling
Top	67.77	67.20	68.45	71.40
Bottom	351.71	350.51	353.22	362.15

FIG. 5. COMPARISON OF WARMING RATES COMPUTATIONS BASED ON CROSS-SECTIONS IN FIG. 1A (PRESENT METHOD) AND ON THE ESFT METHOD (SEE TEXT) FOR (A) 200–294 nm, (B) 294–312 nm, (C) 312–400 nm, AND (D) 400–700 nm.
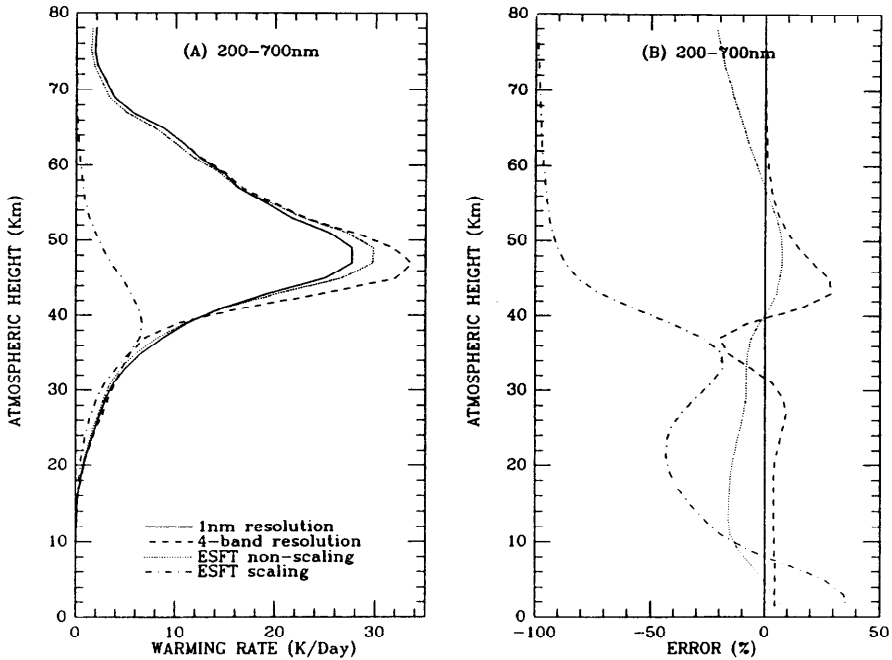
FIG. 6. WARMING RATE COMPARISONS FOR THE RANGE 200–700 nm BASED ON CROSS-SECTIONS IN FIG. 1A
(PRESENT METHOD) AND ON THE ESFT METHOD FOR (A) WARMING RATES AND (B) CORRESPONDING ERRORS.

3.3. Photodissociation rates

In order to illustrate the effect of the resolution on computed photodissociation rates, we show in Fig. 8 profiles of that rate for ozone computed with different spectral resolution. We see that for this particular

FIG. 7. COMPUTING TIME AS A FUNCTION OF SPECTRAL
RESOLUTION

molecule photodissociation rates accurate to within a few percent are obtained by using a 10 nm resolution below 330 nm (Hartley and Huggins bands), while an average over the entire wavelength region from 400 to 700 nm yields similar accuracy for the Chappuis band. This means that we have reduced the integration over wavelength to just a few monochromatic calculations. Although the accuracy of the integration in equation (6) for a given spectral resolution will depend on the structure of the photoabsorption cross-section for the species under consideration, the results in Fig. 8 indicate that a quite coarse spectral resolution should in general yield adequate results. Finally, we note that the photolysis rates given in Fig. 8 agree well with calculations by Luther and Gelinas (1976) and curves provided in Brasseur and Solomon (1984).
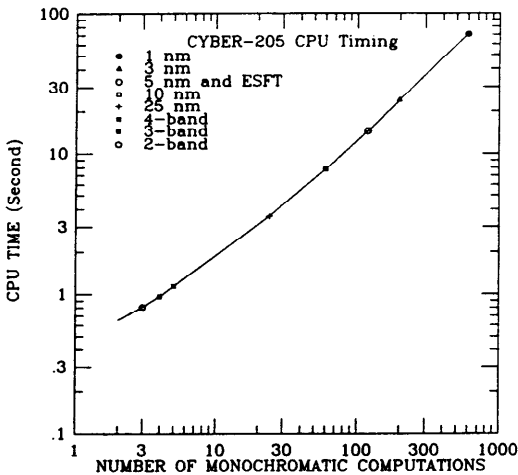
3.4. Integration over spectral regions—u.v. doses

The use of model calculations to quantify the effect of atmospheric ozone changes on the amount of radiation received by the biosphere, is a matter of great current interest, mainly because of the lack of measurements directly linking atmospheric ozone content and transmitted u.v. radiation (Stamnes et al., 1988a). Atmospheric transmission at u.v. wavelengths depends not only on the total ozone content, but also
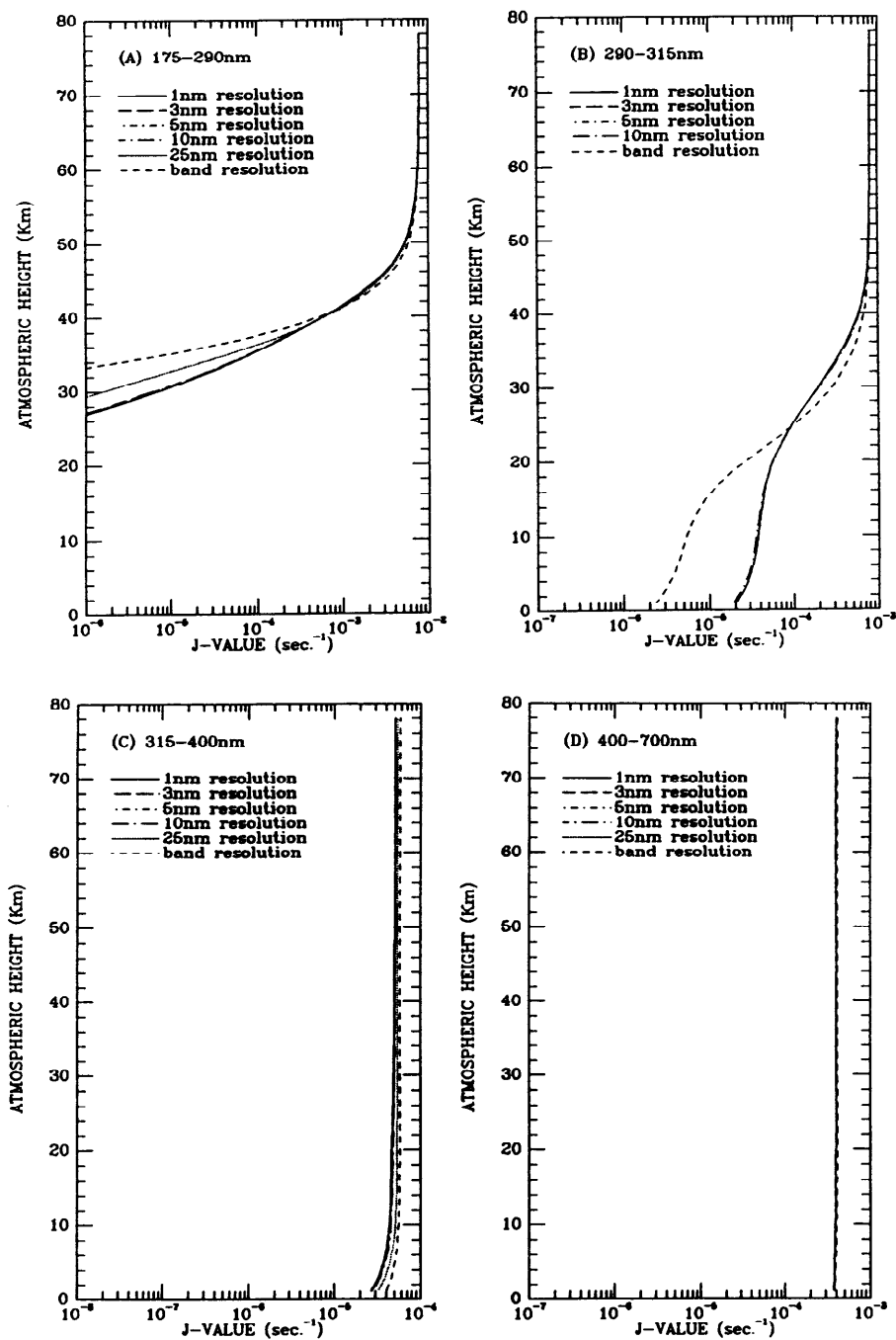
FIG. 8. PHOTOLYSIS RATE FOR OZONE IN VARIOUS SPECTRAL RESOLUTIONS; (A) 175–290 nm, (B) 290–315 nm
(U.V.B), (C) 315–400 nm (U.V.A), AND (D) 400–700 nm (CHAPPUIS BAND).

TABLE 3. COMPUTATIONS OF TRANSMITTED FLUXES (W m^{-2}) AT THE SURFACE FOR DIFFERENT SPECTRAL
RESOLUTIONS

	1 nm	3 nm	5 nm	10 nm	25 nm	Band
175–290 nm	—	—	—	—	—	—
290–315 nm	0.62	0.61	0.59	0.54	0.01	0.01
315–400 nm	37.89	37.87	37.87	37.85	37.71	37.21
400–700 nm	273.66	273.66	273.66	273.66	273.65	273.16
175–700 nm	312.16	312.14	312.12	312.04	311.37	310.38

on the vertical distribution of ozone. In fact, a recent study by Bruhl and Crutzen (1989) shows that an increase in tropospheric ozone of an amount smaller than a corresponding decrease in stratospheric ozone (so that the total column is depleted), will lead to a reduction of transmitted u.v. radiation in spite of the fact that total column ozone is reduced. The reason for this reduction in transmission is due to the increased pathlength of photons in the troposphere (and thereby increased absorption) caused by multiple scattering. It is therefore important to have available accurate and efficient means for computing the amount of u.v. radiation penetrating through the atmosphere. In Table 3 we show the effect of changing the spectral resolution on the computed transmitted irradiance for the four spectral ranges and the full range (175–700 nm). An accuracy better than 10% in the u.v.B region (290–315 nm) requires a spectral resolution slightly better than 10 nm. We may, however, treat the u.v.A region (315–400 nm) as a single band, and yet have an accuracy better than 2%. For the Chappuis band (400–700 nm) the situation is even better: a single-band integration yields an accuracy better than 0.2%.

Similarly in Table 4 we show the sensitivity of u.v.

dose calculations to spectral resolution. We present results for four different types of action spectra: a generalized DNA damage spectrum (Setlow, 1974), a generalized plant damage spectrum (Caldwell et al., 1986), a weighting spectrum for erythema (McKinlay and Diffey, 1987), and the response spectrum of a u.v. meter which was designed to approximate the erythemal (sunburn) response of Caucasian skin [Robertson–Berger or R–B meter, Robertson (1975)]. These action spectra are shown in Fig. 9. Table 4 shows that in the u.v.B region a 10 nm resolution yields an error less than 3% for the action spectra of erythemal and plant response, while a resolution better than 5 nm is required to yield a similar accuracy for the R–B meter and, in particular, the DNA response. In the u.v.A region a 10 nm resolution provides an accuracy of about 5%. Inspection of Fig. 9 shows that these results are as expected based on the shapes of the various action spectra.

4. DISCUSSION

As already mentioned the cross-section for molecular oxygen in Fig. 1 includes only the Herzberg con-

TABLE 4. SENSITIVITY OF U.V. DOSE (10^{-3} W m^{-2}) COMPUTATIONS TO DIFFERENT SPECTRAL RESOLUTIONS

(a) u.v.B: 290–315 nm

	1 nm	3 nm	5 nm	10 nm	25 nm	Band
Erythema	7.280	7.318	7.412	7.476	1.132	1.132
Plant	2.759	2.802	2.900	2.706	0.435	0.435
R–B meter	72.88	72.12	70.68	63.89	2.048	2.048
DNA	0.277	0.232	0.244	0.294	0.166	0.166

(b) u.v.A: 315–400 nm

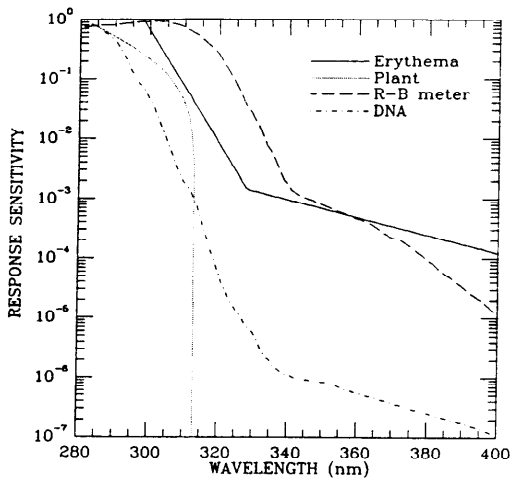|	1 nm	3 nm	5 nm	10 nm	25 nm	Band
Erythema	6.467	6.492	6.520	6.738	7.546	9.044
Plant	—	—	—	—	—	—
R–B meter	97.91	98.52	98.73	103.7	126.8	164.6
DNA	0.032	0.032	0.033	0.036	0.044	0.057

FIG. 9. ACTION SPECTRA USED TO COMPUTE U.V. DOSES FOR
SEVERAL BIOLOGICAL PROCESSES.

tinuum in the spectral range 175–200 nm. The major
absorption here is, however, the Schumann–Runge
bands which may pose considerable difficulties to
realistic modeling. The cross-sections for the
Schumann–Runge bands of Yoshino *et al.* (1983)
were recommended for use in stratospheric modeling
by WMO (1985) with the caveat "these data, obtained
at a temperature of 300 K, are not currently in a form
that is directly applicable to atmospheric studies ...".
Furthermore, the Schumann–Runge band cross-
section varies quite rapidly over small wavelength
intervals. It is also temperature and thereby altitude
dependent due to Doppler broadening. Lacking
a convenient set of cross-section data suitable for
our purposes, we have intentionally omitted the
Schumann–Runge band system from consideration in
this paper.

Since the use of the extraterrestial solar flux in equa-
tion (7) provides good results, one might speculate if
use of the attenuated solar beam could yield an even
better approximation. Such a weighting would make
the effective cross-sections altitude dependent, but this
is not a problem because the optical depth is the true
independent variable, and only a modification of its
altitude dependence is required. The inclusion of an
altitude dependent cross-section is easily accom-
modated in a model such as ours, and it is conceivable
that such a refinement of the approach described in
this paper may lead to even faster computation and
more accurate results. We certainly feel that this topic
would be well worth pursuing. We recommend, how-
ever, that such a study be combined with an inves-

tigation of the effects of temperature (and thereby
altitude) dependence of the photoabsorption cross-
sections for the key trace species important in the
ozone chemistry, in general, and for the Schumann–
Runge band system discussed above, in particular.

5. SUMMARY AND CONCLUSION

We have presented a very efficient method for com-
puting atmospheric warming and photolysis rates. In
this scheme the integration over wavelength is reduced
to a small number of monochromatic (or pseudo-
gray) problems by weighting the cross-sections with
the solar flux across appropriately chosen spectral
intervals. We have shown that for the spectral range
175–700 nm, warming rates with errors less than 20%
throughout the troposphere and stratosphere are
obtained by utilizing only four effective mono-
chromatic calculations. In general, the computations
of photolysis rates accurate to within a few percent
(which is the order of the ozone trends being studied,
NASA, 1988) would require only a few mono-
chromatic calculations. To estimate u.v. dose in the
u.v.B region (290–315 nm) a 10 nm resolution yields
an error less than 3% for the action spectra of
erythemal and plant response, while a resolution
better than 5 nm is required to yield similar accuracy for
the DNA response. In the u.v.A region (315–400 nm)
a 10 nm resolution provides an accuracy of about 5% .

By comparing our present scheme with the com-
monly used exponential-sum-fitting-of-transmissions
(ESFT) method, we conclude that (1) pressure and
temperature scaling of ozone absorber amount is
definitely inappropriate in the u.v. and visible part of
the spectrum, (2) good agreement between our present
method and the ESFT technique is obtained when
such scaling is avoided, and (3) the present method
based on weighting the cross-sections with the solar
flux, is more than 10 times faster than the ESFT-
technique for the same accuracy.

In summary, we have demonstrated that the present
scheme provides a very efficient means of computing
atmospheric warming and photolysis rates; because
of its efficiency, this scheme can readily be included in
large-scale climate and photochemical models. The
distinct advantage of the present method compared
with various existing parameterizations of solar radi-
ation in large-scale models, is that cloud and haze
layers can be easily accommodated at any level in
the atmosphere (cf. Tsay *et al.*, 1989). In fact, our
approach would allow for a more realistic treatment
of cloud microphysics in climate models than is pre-
sently available, and could thereby lead to a better

understanding as well as improved assessment of the role of cloud/radiation/climate feedback mechanisms, which is a matter of vexing concern in the climate modeling community (cf. e.g. Mitchell, 1989).

REFERENCES

Brasseur, G. and Solomon, S. (1984) *Aeronomy of the Middle Atmosphere*. D. Reidel, Dordrecht.

Bruhl, C. and Crutzen, P. J. (1989) On the disproportionate role of tropospheric ozone as a filter against solar UV-B radiation. *Geophys. Res. Lett.* **16**, 703.

Caldwell, M. M., Camp, L. B., Warner, C. W. and Flint, S. D. (1986) Action spectra and their key role in assessing the biological consequences of solar u.v.B radiation change, in *Stratospheric Ozone Reduction, Solar Ultraviolet Radiation and Plant Life* (Edited by Worrest, R. C. and Caldwell, M. M.), pp. 87–111. Springer, Berlin.

Chandrasekhar, S. (1960) *Radiative Transfer*. Dover, New York.

Dahlback, A., Henriksen, T., Larsen, S. H. H. and Stamnes, K. (1989) Biological UV-doses and the effect of an ozone layer depletion. *Photochem. Photobiol.* **49**, 621.

Frederick, J. E. and Lubin, D. (1988) The budget of biologically active ultraviolet radiation in the Earth-atmosphere system. *J. geophys. Res.* **93**, 3825.

Goody, R. M. and Yung, Y. L. (1989) *Atmospheric Radiation*. Oxford University Press, New York.

Kondratyev, K. Y. (1969) *Radiation in the Atmosphere*. Academic, New York.

Liou, K.-N. (1980) *An Introduction to Atmospheric Radiation*. Academic, New York.

Liou, K.-N. and Ou, S.-C. (1989) The role of microphysical processes in climate: an assessment from a one-dimensional perspective. *J. geophys. Res.* **94**, 8599.

Luther, F. M. and Gelinas, R. J. (1976) Effect of molecular multiple scattering and surface albedo on atmospheric photodissociation rates. *J. geophys. Res.* **81**, 1125.

Madronich, S. (1987) Photodissociation in the atmosphere: 1. Actinic flux and the effects of ground albedo and clouds. *J. geophys. Res.* **92**, 9740.

McKinlay, A. F. and Diffey, B. L. (1987) A reference action spectrum for ultra-violet induced erythema on human skin, in *Human Exposure to Ultraviolet Radiation: Risks and Regulations* (Edited by Passchier, W. F. and Bosnajakovic, B. F. M.), p. 83. Elsevier, Amsterdam.

Meier, R. R., Andersons, D. E., Jr. and Nicolet, M. (1982)

Radiation field in the troposphere and stratosphere from 240 to 1000 nm, I. General analysis. *Planet. Space Sci.* **30**, 923.

Mitchell, J. F. B. (1989) The "Greenhouse" effect and climate change. *Rev. Geophys.* **27**, 115.

Molina, L. T. and Molina, M. J. (1986) Absolute absorption cross section of ozone in the 185- to 350-nm wavelength range. *J. geophys. Res.* **91**, 14501.

NASA: Ref. Publ. 1208 (1988) Present state of knowledge of the upper atmosphere 1988: an assessment report.

Nicolet, M. (1989) Solar spectral irradiances with their diversity between 120 and 900 nm. *Planet. Space Sci.* **37**, 1249.

Nicolet, M., Meier, R. R. and Andersons, D. E., Jr. (1982) Radiation field in the troposphere and stratosphere from 240 to 1000 nm, II. Numerical analysis. *Planet. Space Sci.* **30**, 935.

Robertson, D. F. (1975) The sunburn unit for comparison of variation of erythemal effectiveness (Edited by Nachtwey, D. S., Caldwell, M. M. and Biggs, R. H.), in *Impacts of Climatic Change on the Biosphere*, part 1, Ultraviolet Radiation Effects. Monograph 5. Climatic Impact Assessment program, U.S. Dept Transportation report No. DOT-TST-75-55, NTIS, Springfield, Virginia.

Scotto, J., Cotton, G., Urbach, F., Berger, D. and Ferris, T. (1988) Biologically effective ultraviolet radiation: surface measurements in the United States, 1974 to 1985. *Science* **238**, 762.

Setlow, R. B. (1974) The wavelengths in sunlight effective in producing skin cancer: a theoretical analysis. *Proc. natn. Acad. Sci. U.S.A.* **71**, 3363.

Stamnes, K. (1986) The theory of multiple scattering of radiation in plane parallel atmospheres. *Rev. Geophys.* **24**, 299.

Stamnes, K., Henriksen, K. and Ostensen, P. (1988a) Simultaneous measurement of UV radiation received by the biosphere and total ozone amount. *Geophys. Res. Lett.* **15**, 784.

Stamnes, K., Tsay, S.-C., Wiscombe, W. and Jayaweera, K. (1988b) Numerically stable algorithm for discrete-ordinate-method radiative transfer in multiple scattering and emitting media. *Appl. Optics* **27**, 2502.

Tsay, S.-C., Jayaweera, K. and Stamnes, K. (1983) Dependence of radiative properties of arctic stratus clouds on cloud microstructure. *Geophys. Res. Lett.* **12**, 1188.

Tsay, S.-C., Stamnes, K. and Jayaweera, K. (1989) Radiative energy budget in the cloudy and hazy Arctic. *J. atmos. Sci.* **46**, 1002.

Tsay, S.-C., Stamnes, K. and Jayaweera, K. (1990) Radiative transfer in stratified atmospheres: description and development of a unified model. *J. Quant. Spectrosc. Radiat. Transfer* **43**, 133.

World Meteorological Organization (1985) Global ozone research and monitoring project, Rep. No. 16, Atmospheric Ozone 1985, 1.

Yoshino, K., Freman, D. E., Esmond, J. R. and Parkinson, W. H. (1983) High resolution absorption cross section measurements and band oscillator strengths of the (1,0)–(12,0) Schumann–Runge bands of O_2. *Planet. Space Sci.* **31**, 339.